Cross section measurements of the ^{93}Nb$(p,\gamma)^{94}$Mo reaction at $E_p = 1.4-4.9$ MeV relevant to the nucleosynthetic *p* process

S. Harissopulos, E. Skreti, P. Tsagari, G. Souliotis, P. Demetriou, and T. Paradellis
Institute of Nuclear Physics, NCSR "Demokritos," 153.10 Aghia Paraskevi, Athens, Greece

J. W. Hammer and R. Kunz
Institut für Strahlenphysik, Universität Stuttgart, Allmandring 3, 70569 Stuttgart, Germany

C. Angulo
Cyclotron Research Center, Université Catholique de Louvain, Chemin du Cyclotron 2, 1348 Louvain la Neuve, Belgium

S. Goriely
Institut d'Astronomie et d'Astrophysique, Université Libre de Bruxelles, Campus de la Plaine, CP-226, 1050 Brussels, Belgium

T. Rauscher
Departement für Physik und Astronomie, Universität Basel, Klingelbergstr. 82, 4056 Basel, Switzerland
(Received 8 June 2001; published 19 October 2001)

In-beam cross section measurements of the ^{93}Nb$(p,\gamma)^{94}$Mo reaction have been carried out at $E_p = 1.4-4.9$ MeV, by using high efficiency high-purity Ge detectors, partly with BGO shields for Compton background suppression. From the resulting cross sections, which lie in the 0.5–300 μb range, astrophysical *S* factors as well as reaction rates have been obtained. By means of the statistical compound nucleus theory of Hauser and Feshbach, cross sections and reactions rates have also been calculated. A good agreement between the experimental data and the theoretical predictions has been found.

DOI: 10.1103/PhysRevC.64.055804 PACS number(s): 25.40.Lw, 26.30.+k, 27.60.+j, 97.10.Tk

I. INTRODUCTION

Cross section measurements of nuclear reactions taking place in stellar environments are of key importance in the modeling of stellar evolution and nucleosynthesis. From such measurements, one obtains the corresponding reaction rates that arise as coefficients in the so-called rate equations (see, e.g., Ref. [1]) that have to be solved in the framework of a model of nucleosynthesis. By means of these equations, one can describe the change of the isotopic abundances in a stellar environment of temperature *T*. Hence, a successful reproduction of the abundances of nuclei by any model of nucleosynthesis requires accurate knowledge of the reaction rates over a wide temperature range, i.e., the cross sections of the involved nuclear reactions have to be known over a certain energy region. This requirement, however, is not fulfilled in the case of the so-called *p* nuclei, a certain class of nuclei heavier than iron, due to the fact that the reproduction of their abundances requires extended reaction network calculations involving more than 20 000 nuclear reactions on about 2000 nuclei in the mass region $12 \leqslant A \leqslant 210$. Obviously, experimental data on the cross sections of all these reactions could hardly be available. Consequently, all the relevant calculations have to rely almost completely on the cross sections predicted by the Hauser-Feshbach (HF) theory [2].

The term *p nuclei* refers to 32 stable neutron-deficient nuclei that, in contrast to all the other nuclei that are heavier than iron, cannot be synthesized by the two neutron capture processes referred to as *s* and *r* processes [3–5]. In fact, a special mechanism, called the *p* process, is assumed by the theory of nucleosynthesis to be responsible for their production. As *p* nuclei lie on the proton-rich side of the stability valley between ^{74}Se and ^{196}Hg, they cannot be produced by neutron capture. Hence, they are taken to originate from the "burning" of preexisting more neutron-rich nuclei at stellar environments of high enough temperature ($T \geqslant 2 \times 10^9$), where photodisintegrations of such nuclei can occur. Such temperature conditions are fulfilled in the O/Ne layers of massive stars during their presupernova phase [6,7] or during their explosion as type II supernovae (SNII) [7–9]. These *p*-process scenarios involve more or less complicated sequences of (γ,n), (γ,p), and (γ,α) reactions.

Although various *p*-process calculations have been successful [7,9–13] in reproducing the abundances of a variety of *p* nuclei, this is not the case for those in the mass region $70 \leqslant A \leqslant 110$. In this region, the relatively large abundances of ^{92}Mo, ^{94}Mo, ^{96}Ru, and ^{98}Ru are severely underpredicted, whereas those of the lighter *p* nuclei ^{74}Se, ^{78}Kr, and ^{84}Sr are systematically overpredicted. These discrepancies could be attributed to uncertainties in the modeling of the preceding *s*-process nucleosynthesis [14] or in the description of the stellar interior [15]. In addition to the importance of the astrophysical modeling, it remains a challenge to test the reliability of the nuclear physics input in the HF model. One of the major problems in this respect is the lack of experimental data. In fact, for the mass region considered, there are seven experimental works reporting on (p,γ) cross section measurements [16–22] and three papers on (α,γ) [23–25]. In some of them, significant discrepancies have been observed between theory and experiment, whereas in others good agreement with the statistical model predictions has been

 ©2001 The American Physical Society

found. Since it remains an open question whether the HF calculations can provide satisfying results, further experimental works, like the present one, are essential.

II. EXPERIMENTAL PROCEDURES

The present measurements have been carried out at the 4 MV single-ended Dynamitron accelerator of the University of Stuttgart, as well as at the 5 MV Van de Graaff tandem accelerator of the Institute of Nuclear Physics of NCSR ''Demokritos,'' Athens. Both accelerators have been calibrated during the experiments by means of the 992 keV resonance of the $^{27}\mathrm{Al}(p,\gamma)^{28}\mathrm{Si}$ reaction.

The experimental setup used during the first set of measurements in Stuttgart, was the same with that described in Ref. [26]. γ spectra were measured by using four large volume high-purity Ge (HPGe) detectors, all shielded with BGO crystals for Compton supression. Three of them had a relative efficiency $\epsilon_r \approx 100\%$, whereas the remaining one had $\epsilon_r \approx 76\%$. The detectors were placed on a rotating table at distances between 12 and 20 cm from the target. By rotating the table by a step of 15° γ-single spectra were taken at eight angles with respect to the beam. In this way, the angular distributions of the γ rays of interest were measured in the energy range $E_p = 2-3$ MeV with a step of 50 keV. The beam current was about 20 μA. The target used was placed at 90° to the beam axis. It was produced by evaporating Nb_2O_5 on a 0.4 mm thick tantalum backing, which was cooled with water during the whole experiment. It should be noted that the use of the Nb_2O_5 target requires corrections for yield contributions from the $^{17}\mathrm{O}(p,p'\gamma)^{17}\mathrm{O}$ reaction occuring in the oxide part of the target (see further below). This problem could be avoided by using a metallic Nb target. However, the use of Nb_2O_5 targets in the beginning of the present measurements was inevitable since the metallic Nb had not been delivered according to the beam time schedule. The thickness of Nb in the Nb_2O_5 target was found to be 126 ± 5 μg/cm^2 by means of an XRF analysis carried out before the measurement. By considering the target stoichiometry (Nb:O = 0.699:0.301) one obtains a target total thickness of 180 ± 6 μg/cm^2, which corresponds to a target thickness ΔE of 20 and 12 keV at a beam energy of 1.5 and 3 MeV, respectively.

In the second set of measurements carried out in Athens, γ spectra were taken by means of one HPGe detector of 80% relative efficiency that was placed either at 55° or at 90° to the beam axis. Two different Nb targets positioned at 45° to the beam axis were used, namely, Nb_2O_5 and a metallic Nb. The latter target was made by electron gun evaporation of metallic niobium of extreme high purity. The fluorine level in the metal was less than 1 ppm. The energy region covered by the measurements using the metallic Nb was from 1.4 to 4.9 MeV. Both targets were on 0.4 mm thick Ta backings, which were cooled with air during the measurements. By using the XRF method, it was found that the thickness of Nb in the Nb_2O_5 target was 106 ± 6 μg/cm^2, i.e., the target had a total thickness of 151 ± 7 μg/cm^2. For the metallic target the XRF analysis yielded a thickness of 371 ± 18 μg/cm^2, which corresponds to $\Delta E = 31$ and 20 keV at proton beam energies of 1.5 and 3 MeV, respectively. According to a Rutherford backscattering (RBS) combined with PIGE and XRF analysis, the stoichiometry of the metallic target was found to be (Nb:O:N:C) = (0.94:0.025:0.025:0.010). The O, N, and C were apparently introduced in the target during the evaporation process, since these elements were not present in the original high purity Nb metal. All targets used in the present work were also checked at the end of all measurements via the XRF technique. No significant deterioration effects were found.

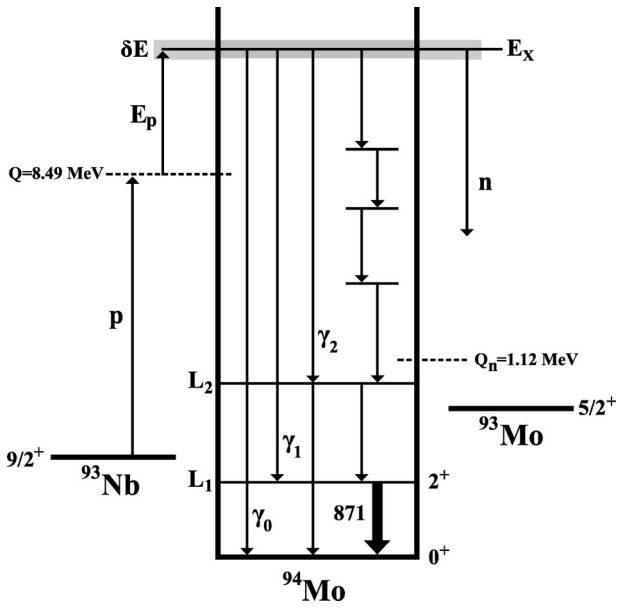

FIG. 1. Simplified level diagram of the ^{94}Mo nucleus.

As already mentioned, in the case of the Nb_2O_5 targets corrections for yield contributions from the $^{17}\mathrm{O}(p,p'\gamma)^{17}\mathrm{O}$ reaction were necessary. The γ rays emitted by the latter reaction have an energy of 871 keV, which coincides with the energy of the $2_1^+ \rightarrow 0_1^+$ transition of the excited ^{94}Mo nuclei produced by the $^{93}\mathrm{Nb}(p,\gamma)$ reaction. The required corrections, which are described in detail in the next section, were performed with additional yield measurements carried out with a WO_3 target. According to the XRF analysis of this target, the thickness of W was found to be 153 ± 5 μg/cm^2. By taking into account the stoichiometry of the WO_3 target, the thickness of its oxide part was 40 ± 1.3 μg/cm^2, which is almost the same as that of the Nb_2O_5 target measured in Athens. During all measurements, the beam current was about 2 μA.

III. DATA ANALYSIS AND RESULTS

In order to obtain the cross section of the $^{93}\mathrm{Nb}(p,\gamma)^{94}\mathrm{Mo}$ reaction, the absolute number of all emitted photons has to be determined first. Hence, one has to derive the absolute yield of all the γ transitions feeding the ground state of the produced ^{94}Mo. This task requires angular distribution measurements of all these γ transitions. As indicated in Fig. 1, where a simplified level diagram of the ^{94}Mo nucleus is sketched, the ground state can be populated by a γ transition directly from the entry state as well as by cascades of γ rays

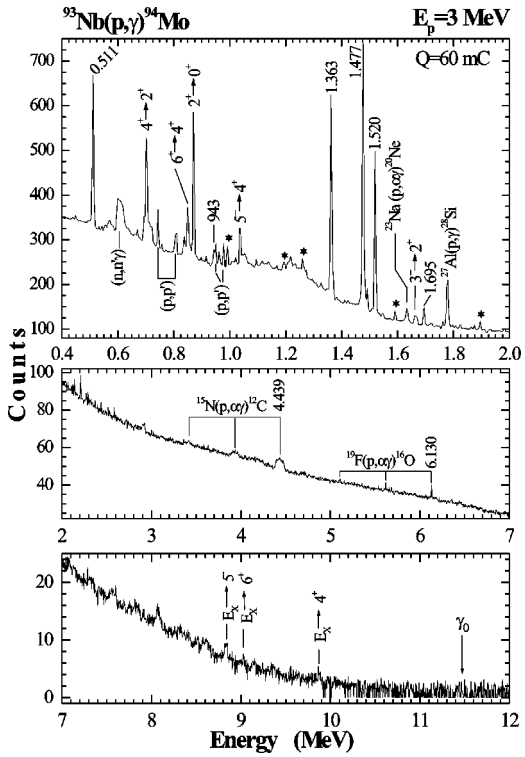

FIG. 2. Typical γ spectrum measured at $E_p=3$ MeV with the metallic Nb target. The strong γ transitions belonging to the ^{93}Nb$(p,\gamma)^{94}$Mo reaction are indicated by the corresponding spins of the initial and final state, whereas some weak γ transitions are labeled with stars. The γ rays from the ''entry state''—with energy $E_X=Q+E_{\text{c.m.}}$—to the lowest-lying 6^+, 5^-, and 4^+ levels are indicated as $E_x\rightarrow 6^+$, $E_x\rightarrow 5^-$, and $E_x\rightarrow 4^+$, respectively. The label γ_0 shows the ''position'' where the γ transition from the ''entry'' to the ground state should appear. As shown in this figure no such γ ray has been observed. The γ rays from the ^{93}Nb$(p,n)^{93}$Mo reaction are indicated by the respective energy. Peaks arising from the (p,p') channel as well as from other ''intruding'' reactions are also shown.

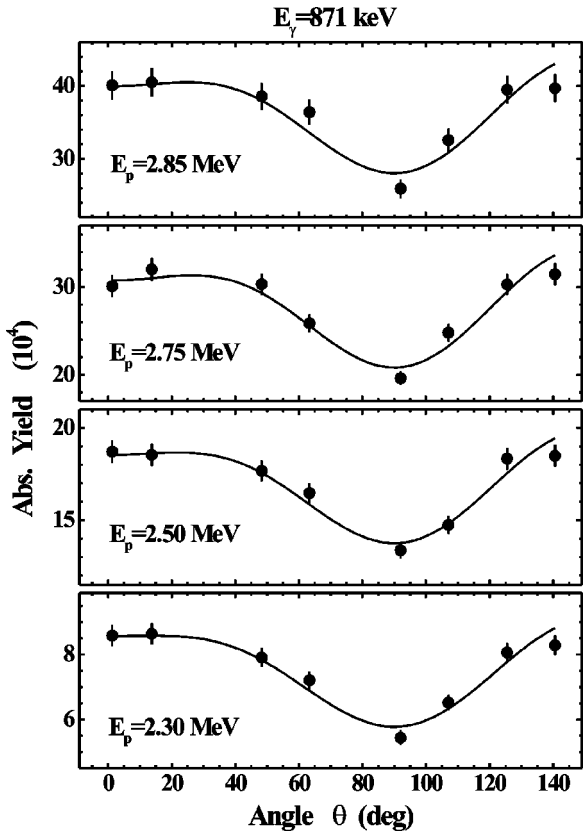

FIG. 3. Typical γ angular distributions of the 871 keV γ transition measured with the 180 μg/cm^2 thick Nb_2O_5 target.

depopulating various excited levels. The former transition is the so-called γ_0 transition having an energy $E_{\gamma 0}=Q_{(p,\gamma)}+E_{\text{c.m.}}$. The direct feeding to the first excited level L_1 or to the second excited level L_2 results in the γ_1 transition or in the γ_2 transition, respectively, and so on. In the present work, as shown in Fig. 2, no γ_0 transition or other γ rays feeding into the ground state have been observed apart from the $2_1^+\rightarrow 0_1^+$ γ transition.

The absence of γ_0 transitions in the reaction studied is more or less expected: From partial wave analysis with an appropriate nucleon-nucleus potential it can be shown that at the relevant beam energies of 1.5–4.5 MeV, only the *s*- and *p*-wave protons have considerable chance of being absorbed by the target nucleus. As the spin of the ground state of the target nucleus ^{93}Nb is $\frac{9}{2}^+$, the spin of the entry states of the produced compound nucleus ^{94}Mo would have values $J=3,4,5,6$. However, their deexcitation would proceed preferably via γ transitions to levels with small spin difference, so γ rays from the entry levels to the ground state ($J_{\text{g.s.}}=0$) are unfavorable.

In view of these findings, it was possible to derive the cross section of the reaction studied from the angular distribution of the $2_1^+\rightarrow 0_1^+$ γ ray only of the ^{94}Mo nucleus. Some typical angular distributions measured at Stuttgart with the Nb_2O_5 target are shown in Fig. 3. Due to time limitations angular distributions were measured at beam energies $E_p=2-3$ MeV only. The analysis of the angular distributions of the 871 keV γ ray yielded a_2 and a_4 coefficients that were statistically constant in the range $E_p=2-3$ MeV. The mean values of the a_2 and a_4 coefficients were found to be $\langle a_2\rangle=0.284(9)$ and $\langle a_4\rangle=-0.118(6)$. Note that the angular distribution measured for the 871 keV γ ray at each beam energy is the sum of the yield Y_{Mo} of the $2_1^+\rightarrow 0_1^+$ γ transition of the ^{94}Mo nucleus and the yield Y_{O} of the 871 keV γ ray from the ^{17}O$(p,p'\gamma)^{17}$O reaction occurring in the oxide part of the Nb_2O_5 target. Consequently, the angular distributions measured in Stuttgart had to be corrected for the yield contribution Y_{O}. In order to perform the necessary corrections additional measurements were carried out in Athens using a second Nb_2O_5 and a WO_3 target with comparable O thickness.

The γ-single spectra were measured at beam energies from 1.7 to 3 MeV using one Ge detector placed at 55° with respect to the beam and at a distance of about 15 cm from the target, which was Nb_2O_5 with a total thickness of 151 ± 7 μg/cm^2. As expected, the analysis of the spectra taken below 2 MeV resulted in yields that exhibited a drastic increase at $E_p=1986$ and 1835 keV, i.e., resonantlike peaks

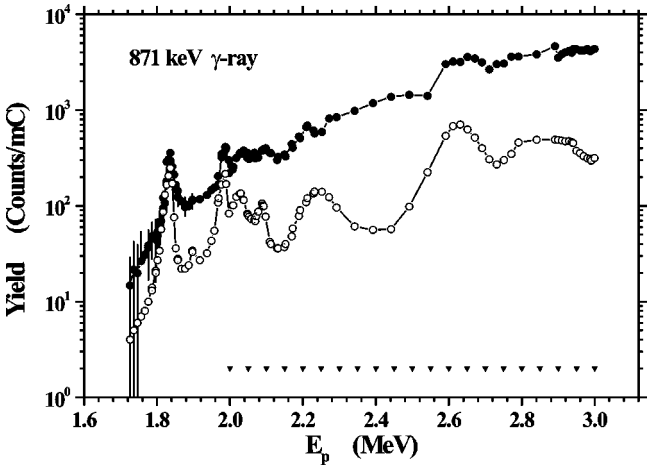

FIG. 4. Yield of the 871 keV γ transition measured with the 151 μg/cm^2 thick Nb_2O_5 target (solid circles), and yield deduced for the 871 keV γ ray arising from the oxide part of the target due to the $^{17}O(p,p'\gamma)^{17}O$ reaction (open circles). The energy points where γ angular distributions were measured are indicated by the triangles.

were observed. The peaks were the result of the $^{17}O(p,p'\gamma)^{17}O$ reaction. Indeed, as reported in Ref. [27], at $E_p=1983(2)$ and 1833(1) keV the latter reaction has two resonances that contribute significantly to the yield of the $2_1^+\rightarrow 0_1^+$ γ transition of ^{94}Mo.

Using the same setup but with a WO_3 target additional γ spectra were measured in order to determine the yield contribution of the 871 keV γ ray from the $^{17}O(p,p'\gamma)^{17}O$ reaction only. According to Ref. [27], the 871 keV γ transition arising from $^{17}O(p,p'\gamma)^{17}O$ reaction is isotropic. Data were obtained in the vicinity of the 1.833 MeV resonance by scanning the energy region $E_p=1.7-2.1$ MeV. At higher energies, data were derived from Sens, Refaei, and Pape [27] by normalizing their excitation function to the yield measured in the present work at the 1.833 MeV resonance. The resulting yield was further normalized to the corresponding O thickness of the Nb_2O_5 target used in Athens. The yield curves measured at 55° with the Nb_2O_5 as well as with the WO_3 target are plotted in Fig. 4. From the resulting data the ratio $R_O(E)$ of the yield of the intruding $^{17}O(p,p'\gamma)^{17}O$ reaction to the total yield measured with the Nb_2O_5 target at 55° was deduced. These ratios served to correct the angular distributions measured in Stuttgart by the following procedure: The yield contribution $Y_O(E)$ of the $^{17}O(p,p'\gamma)^{17}O$ reaction in the Nb_2O_5 data was obtained by multiplying the ratio $R_O(E)$ with the value of the angular distribution at 55°. The resulting $Y_O(E)$ was then subtracted from each data point of the measured angular distribution. The resulting *corrected* angular distribution was further fitted in order to derive the net A_0 a_2, and a_4 coefficients associated with the $2_1^+\rightarrow 0_1^+$ γ transition of the ^{94}Mo nucleus. The total σ_T cross sections were deduced from

$$\sigma_T = A_0 \frac{A}{N_A}\frac{1}{\xi}, \tag{1}$$

where A is the atomic weight of Nb, N_A is Avogadros's number, and ξ is the thickness of Nb in the corresponding target.

TABLE I. Total cross sections σ_T determined from the corrected angular distributions measured at Stuttgart with the 180 μg/cm^2 thick Nb_2O_5 target.

$E_{c.m.}$ (MeV)	σ_T (μb)	$E_{c.m.}$ (MeV)	σ_T (μb)	$E_{c.m.}$ (MeV)	σ_T (μb)
1.989	3.5±0.5	2.340	19.5±2.4	2.689	52±5
2.038	4.4±0.6	2.389	25±3	2.739	58±7
2.090	6.2±0.7	2.440	28±4	2.788	65±7
2.139	7.3±0.8	2.489	31±4	2.839	69±8
2.188	12.0±1.2	2.540	40±5	2.889	66±8
2.239	12.2±1.3	2.575	44±6	2.939	70±9
2.291	15.6±1.2	2.639	49±7	2.989	72±10

The resulting cross sections σ_T given in units of μb are summarized in Table I. The energies in this table are the effective energies in the center-of-mass system that were derived by using appropriate stopping powers [28].

The analysis of the corrected angular distributions yielded new values for the a_2 and a_4 coefficients, which, however, are still statistically constant in the energy range 2–3 MeV, with mean values $\langle a_2\rangle=0.315(10)$ and $\langle a_4\rangle=-0.181(9)$ (see Fig. 5). Based on this fact, it was further assumed that the angular distributions of the $2_1^+\rightarrow 0_1^+$ γ transition of the ^{94}Mo nucleus at $E_p\leqslant 2$ MeV and $E_p\geqslant 3$ MeV would not deviate significantly from those measured at $E_p=2-3$ MeV, i.e., they could also be described by

$$W(\theta)=A_0[1+0.315(10)P_2(\cos\theta)-0.181(9)P_4(\cos\theta)]. \tag{2}$$

Further measurements were carried out with metallic Nb, which was delivered in the meantime by the manufacturer, in order to avoid any uncertainties arising from the intruding

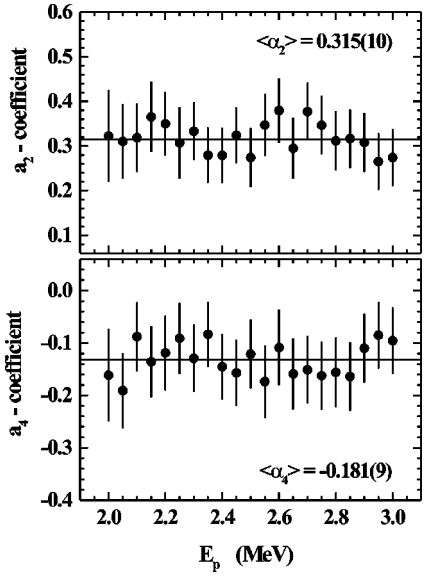

FIG. 5. a_2 and a_4 coefficients resulting from the angular distributions obtained for the 871 keV γ ray after the yield corrections attributed to the intruding $^{17}O(p,p'\gamma)^{17}O$ reaction. The straight solid lines indicate the corresponding mean values.

$^{17}O(p,p'\gamma)$ reaction. γ spectra were measured at beam energies from 1.4 to 4.9 MeV by placing the Ge detector at 90° to the beam and at a close distance ($\approx$4 cm) to the target. The latter was placed at an angle of 45° with respect to the beam. From the analysis of the resulting spectra, the yield of the 871 keV γ transition of ^{94}Mo was determined in the above energy region. The yield obtained was then corrected by the known angular distribution of the $2_1^+ \rightarrow 0_1^+$ γ transition, taking into account the finite solid angle sustained by the detector-target assembly. After calculation of the effective bombarding energy, the yield data were transformed to cross sections by normalization to the Nb_2O_5 angular distribution data. For this procedure, an effective single normalization factor was derived by averaging several yield ratio points at effective energies between 2.3 and 2.5 MeV of the metallic Nb data to the cross sections obtained from the angular distribution data. In this energy interval, the corrections of the Nb_2O_5 data due to the $^{17}O(p,p'\gamma)$ reaction are significantly small (see Fig. 4). It should be noted that the latter normalization procedure was additionally checked by correcting the yield data for the absolute detector efficiency, which was determined using various calibrated sources, thus deriving independent $W(\theta=90°)$ values for the metallic Nb target. These were found to coincide within 5% with those determined from the angular distribution data obtained with the Nb_2O_5 target. The resulting cross sections are given in Table II. The corresponding astrophysical S factors have been calculated by using

$$S(E)=\sigma_T(E)Ee^{2\pi\eta}, \tag{3}$$

where η is the Sommerfeld parameter and $\sigma_T(E)$ is the total cross section at a center-of-mass energy E. The results are included in Table II.

TABLE II. Total cross sections σ_T and astrophysical S factors S determined in the present work. The cross-section values having an error of less than 5% are the means of at least two independent measurements.

$E_{\text{c.m.}}$ (MeV)	σ_T (μb)	S (10^5 MeV b)	$E_{\text{c.m.}}$ (MeV)	σ_T (μb)	S (10^5 MeV b)
1.422	0.05±0.01	349±70	3.093	92±8	26±2
1.462	0.08±0.01	360±45	3.133	108±9	27±2
1.502	0.12±0.02	355±59	3.173	114±9	25±2
1.542	0.16±0.02	316±39	3.192	120±10	25±2
1.582	0.20±0.02	268±27	3.232	121±10	22±2
1.622	0.28±0.02	258±18	3.272	125±10	20±2
1.662	0.38±0.01	245±7	3.311	130±10	18.3±1.4
1.702	0.45±0.03	205±14	3.351	149±7	18.5±0.9
1.741	0.68±0.07	224±24	3.391	145±7	16.0±0.8
1.781	0.89±0.09	212±21	3.430	154±7	15.2±0.7
1.821	1.6±0.1	279±17	3.470	147±12	12.9±1.1
1.861	1.8±0.1	207±13	3.510	157±12	12.4±0.9
1.901	2.1±0.1	203±10	3.549	138±12	9.8±0.9
1.941	3.0±0.2	218±15	3.589	136±11	8.6±0.7
1.981	3.9±0.2	216±11	3.648	124±10	6.7±0.6
2.020	4.1±0.2	205±9	3.688	95±9	4.6±0.4
2.060	5.3±0.2	175±7	3.748	92±9	3.9±0.4
2.100	6.4±0.2	160±5	3.787	93±9	3.5±0.3
2.140	7.5±0.2	152±4	3.827	78±8	2.7±0.3
2.179	10.5±0.4	169±7	3.966	72±6	1.8±0.2
2.219	11.3±0.4	144±5	4.005	93±6	2.1±0.2
2.259	13.7±0.5	140±5	4.045	66±5	1.4±0.1
2.299	15.7±0.5	129±4	4.084	78±5	1.5±0.1
2.339	20.0±0.8	133±5	4.124	79±5	1.38±0.09
2.378	22.0±0.8	120±4	4.144	74±5	1.24±0.08
2.418	26.0±0.8	116±4	4.183	76±6	1.17±0.09
2.498	30±1	87±2	4.223	74±6	1.05±0.09
2.537	38±2	86±4	4.263	95±7	1.24±0.09
2.577	40±3	80±6	4.302	82±7	0.99±0.08
2.617	45±3	79±5	4.342	80±6	0.89±0.07
2.656	50±2	78±3	4.382	77±7	0.79±0.07
2.696	56±2	69±3	4.421	89±8	0.84±0.08
2.736	57±2	61±2	4.461	93±8	0.82±0.07
2.776	54±2	49±2	4.500	106±8	0.86±0.07
2.815	60±2	47±2	4.540	98±8	0.74±0.06
2.855	65±3	43±2	4.580	122±9	0.86±0.06
2.895	64±3	37±2	4.619	161±12	1.05±0.08
2.934	66±3	33±2	4.659	142±11	0.86±0.07
2.974	66±4	28±2	4.718	126±10	0.69±0.06
2.994	75±5	30±2	4.758	196±13	1.00±0.07
3.014	81±6	30±2	4.797	273±23	1.31±0.11
3.053	92±8	30±3			

IV. DISCUSSION

The cross sections measured in the present work are compared with the predictions of the HF compound nucleus theory. In Sec. IV A a brief description of the theory is presented while in Sec. IV B the theoretical calculations are compared with the measured (p,γ) cross sections.

A. Theory of compound nucleus emission

Nuclear reactions occurring at energies up to several MeV are known to proceed through the formation and decay of a compound nucleus system. Absorption of the incident particle leads to the formation of the ''compound nucleus.'' After reaching equilibrium the compound system eventually decays to various states independent of the entrance channel. The probability of decay into one of the decay channels is described by the theory of Hauser and Feshbach [2] and is given by

$$\sigma_{\alpha\beta}=\pi\lambda\!\!\!^{-2}_{\alpha}\frac{1}{(2I+1)(2i+1)}\sum_{J^\pi}(2J+1)\frac{T_\alpha^{J^\pi}T_\beta^{J^\pi}}{\Sigma_{\alpha'}T_{\alpha'}^{J^\pi}}, \tag{4}$$

where α and β denote the entrance and decay channels, respectively, I and i are the target and projectile spins, respectively, and $T_{\alpha,\beta}^{J^\pi}$ are the transmission coefficients, summed over all orbital and channel spins to give the total transmission coefficient for the formation of the compound nucleus in the state J^π. The HF formalism can be applied when the

number of levels in the contributing energy window of the compound nucleus is sufficiently large, and in such cases one uses averaged transmission coefficients obtained from an integral over a specified level density. Hence, for example, the denominator in Eq. (4.1) is given by

$$\sum_{\alpha} T_{\alpha}^{J^{\pi}} = \sum_{\alpha}{}' T_{\alpha}^{J^{\pi}} + \sum_{I\alpha} \int \omega_I(U) T_{\alpha}^{J^{\pi}}(E_{\alpha}) dE_{\alpha}, \qquad (5)$$

where $\omega_I(U)$ is the density of levels of spin I in the residual nucleus. The Σ' indicates that the sum is taken over only those channels leading to the first few discrete levels in the residual nucleus; all other channels are included in the integrals over the excitation energy E_{α} of the residual nucleus.

The two main quantities that govern compound nucleus emission are the transmission coefficients and the nuclear level densities of the residual nuclei. The transmission coefficients for particle emission can be calculated from the appropriate optical model potentials. The photon transmission function is calculated assuming the dominance of dipole transitions in the photon channel. The electric- and magnetic-dipole [giant dipole resonance (GDR)] transition strength functions are usually described by a Lorentz-type function, where the energies and widths are determined by experimental data, where they exist, or by appropriate parametrizations. The nuclear level densities can be derived from phenomenological models leading to simple analytical formulas but only after drastic approximations are made. Alternatively, they can be obtained from microscopic calculations taking into account the discrete structure of the single-particle spectra associated with realistic effective potentials. The latter treat shell, pairing, and deformation effects consistently, whereas in the former they are considered by means of empirical corrections. However, for practical applications, both types of nuclear level density formulas are often renormalized on existing experimental information (low-lying levels and *s*-wave neutron resonance spacings) for each nucleus.

One should emphasize that the uncertainties involved in any HF cross-section calculation are not related to the theory of compound nucleus emission itself, but rather to the uncertainties associated with the evaluation of the nuclear properties entering the calculations. It is therefore of paramount importance to compare the effects of different nuclear inputs over a wide range of nuclei and a broad range of energies.

B. Cross section calculations

In this section we compare the results of the calculations with the ^{93}Nb$(p,\gamma)^{94}$Mo cross sections measured in the present work. Furthermore, we investigate the sensitivity of the theoretical results on two main nuclear ingredients of the HF calculations, namely, (a) the nuclear level density (NLD) and (b) the nucleon-nucleus optical model potential (OMP). The effects due to the α-nucleus OMP and the GDR transmission function shall not be discussed in this paper, since they have been found to be insignificant for the reaction studied.

The HF calculations presented here have been performed by two statistical model codes: MOST [29] and NON-SMOKER [30]. Both codes include all available experimental information on nuclear masses, deformation, spectra of low-lying states, and giant dipole energies. Different predictions are used in both codes for the global nucleon and α-particle OMP's, as well as for nuclear level densities. Details on the codes and the nuclear physics input can be found in the above-mentioned references.

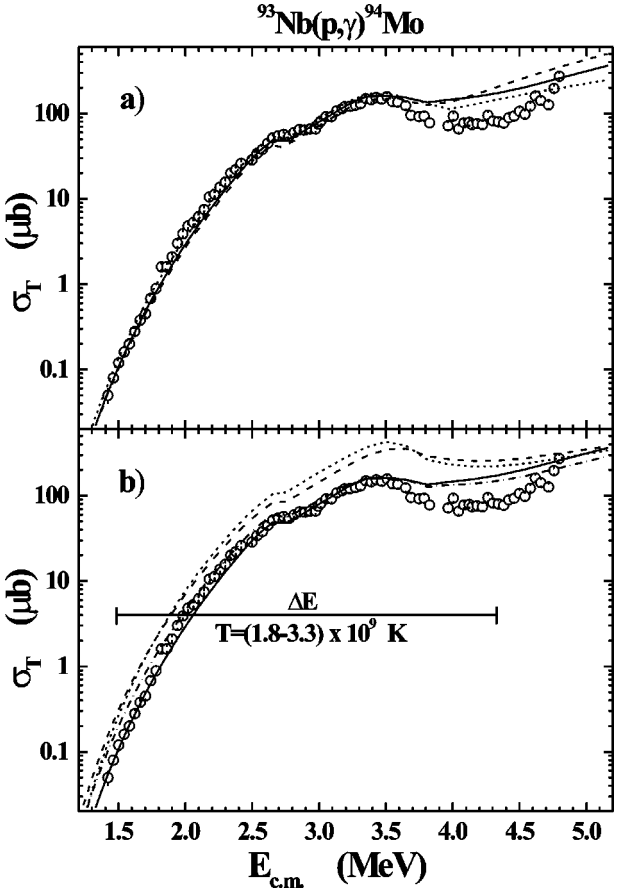

FIG. 6. Total cross sections of the ^{93}Nb$(p,\gamma)^{94}$Mo reaction measured in the present work (open circles) compared with the predictions of the statistical model under different assumptions on (a) nuclear level densities and (b) optical model potentials (see also text). ΔE indicates the energy region corresponding to those stellar temperatures T that are relevant to the p process.

1. Nuclear level densities

Three different nuclear level densities are used to calculate HF reaction cross sections, and the results are compared with the experimental data in Fig. 6(a). The solid line denotes the NLD derived from microscopic statistical calculations based on a Hartree-Fock-BCS level scheme and pairing force [31,32], while the dashed line denotes the microscopic NLD obtained with the ETFSI ground-state structure properties [33]. Both calculations were carried out with the MOST code. The dotted line corresponds to the NLD obtained from the backshifted Fermi-gas model, implemented in the NON-SMOKER code as given in Ref. [34] using microscopic mass correction from the finite range droplet model [35]. The nucleon-nucleus OMP used by both codes is that of Jeu-

kenne, Lejeune, and Mahaux [36]. All three calculations give almost identical results and are in good agreement with the data apart from the higher energies ($E \geqslant 3.5$ MeV), where deviations appear between theory and experiment, and also between the theoretical curves. At the energies measured in this work, the γ and neutron channels dominate over all other emission channels. The differences observed in Fig. 6(a) can thus be attributed to the differences in the NLD predictions for the nuclei ^{94}Mo and ^{93}Mo, related to the channels mentioned above. In principle, the NLD's can be constrained at specific energies using the experimental information, such as low-lying experimental states and *s*-neutron resonance spacings. However, for the nucleus ^{94}Mo associated with the photon emission channel, there are no data on the *s*-wave neutron resonance spacings at the neutron separation energy. Therefore, it is not possible to apply a renormalized NLD that might resolve the discrepancies observed between theory and experiment in the high-energy region.

2. Nucleon-nucleus optical model potentials

In Fig. 6(b) the HF cross sections calculated using the nucleon-nucleus OMP's of (i) Jeukenne, Lejeune, and Mahaux [36] (solid line), (ii) Becchetti and Greenlees [37] (dotted line), and (iii) Bauge, Delaroche, and Girod [38] (dashed line) are compared with the measured data. The calculations were performed by the code MOST using the microscopic Hartree-Fock-BCS nuclear level density of Refs. [31, 32]. The OMP of Jeukenne, Lejeune, and Mahaux, based on microscopic infinite nuclear matter calculations applied with the local density approximation is able to describe the data well at the energies measured in this experiment. On the other hand, both the global OMP of Becchetti and Greenlees and the microscopic potential of Bauge, Delaroche, and Girod lead to an overprediction of the data. The former was obtained by fitting to elastic scattering data at energies above 10 MeV and therefore it is not surprising to see a discrepancy in the lower energy region measured in this work. The latter has been derived in a similar manner as the OMP of Jeukenne, Lejeune, and Mahaux, with a further extension up to energies 200 MeV. In addition, the real and imaginary parts of the OMP have been normalized to reproduce an extensive set of elastic and inelastic scattering data. From the results in Fig. 6(b), however, it appears that this OMP is unable to describe the cross sections measured in this work. The three optical potentials give results that differ over the whole energy range. The HF calculations are extremely sensitive to both proton and neutron transmission coefficients, since at incident energies $E \geqslant 1.2$ MeV the neutron channel opens and starts competing with the γ channel. This observation is further confirmed by the results obtained using the Bauge, Delaroche, and Girod proton-nucleus OMP and the Jeukenne, Lejeune, and Mahaux OMP for the neutron channel (dot-dashed line). The agreement with experiment is significantly improved, with respect to the dashed line, in the high-energy region where the neutron channel is important. In the low-energy region, however, where the neutron channel is still weak compared with the γ channel, the results are comparable to those obtained using the Bauge, Delaroche, and Girod OMP for protons and neutrons. The major difference observed in Fig. 6(b) between the Jeukenne, Lejeune, and Mahaux and the Bauge, Delaroche, and Girod predictions therefore originate from the 4% renormalization of the real (neutron and proton) potential at low energies. The present data are particularly sensitive to both neutron- and proton-nucleus OMP and represent an interesting test case for optimizing global OMP parametrizations.

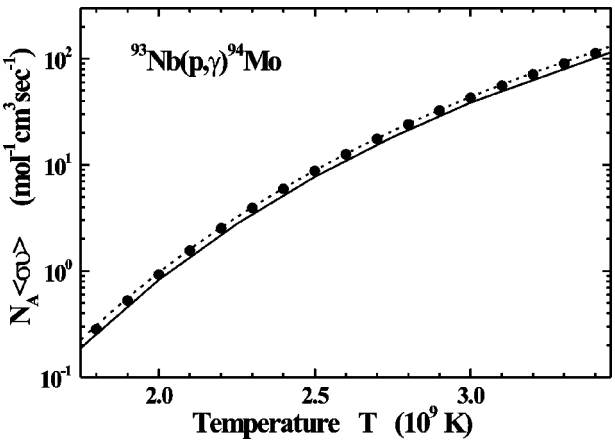

FIG. 7. Rates of the ^{93}Nb$(p,\gamma)^{94}$Mo reaction vs temperature determined in the present work (solid circles) and predicted by MOST (solid line) and NON-SMOKER (dotted line).

C. Reaction rates

p-process nucleosynthesis is assumed to take place in stellar environments where temperatures between 1.8×10^9 and 3.3×10^9 K are maintained for about 1 s. These temperature limits correspond to proton beam energies in the Gamow energy window ranging from 1.48 to 4.32 MeV. This region was completely covered in the present work. Therefore, the reaction rates for different temperatures were calculated by

$$\langle \sigma v \rangle = \left(\frac{8}{\pi \mu} \right)^{1/2} \frac{N_A}{(kT)^{3/2}} \int_0^\infty \sigma(E) E \exp\left(- \frac{E}{kT} \right) dE, \quad (6)$$

where $\sigma(E)$ are the cross sections determined experimentally, kT is the thermal energy, E is the center-of-mass energy, and N_A is Avogadro's number. The results are compared in Fig. 7 with the theoretical predictions obtained by MOST using the microscopic NLD of Refs. [31, 32] and by NON-SMOKER using the NLD of Ref. [34]. In both cases the OMP of Ref. [36] was used.

As can be seen in Fig. 7, the data (solid circles) are in very good agreement with the theoretical curves, particularly with that of NON-SMOKER (dotted line). However, one should stress that the reaction rates shown in Fig. 7 are ground-state reaction rates. In order to derive stellar rates that are relevant for astrophysical calculations one has to additionally consider proton captures by target nuclei in thermally populated excited states. The corresponding rates can be found in Refs. [29, 30].

V. CONCLUSIONS

In the present work, the total cross section of the ^{93}Nb$(p,\gamma)^{94}$Mo reaction was measured at 104 beam energies

ranging from 1.4 to 4.9 MeV by using in-beam γ-spectroscopy techniques combined with HPGe detectors of very high efficiency in order to test the predictions of various statistical model calculations in the $A \approx 90$ mass region where experimental data are rare. The data were compared with theoretical calculations carried out using the statistical model codes MOST and NON-SMOKER.

Overall, all calculations gave almost identical results in very good agreement with experiment, independent of the NLD used. Some discrepancies appear though, at energies above $\approx$3.5 MeV due to uncertainties in the determination of NLD's in this energy region. The agreement found at energies up to 3.5 MeV, however, holds when the nucleon-nucleus OMP of Jeukenne, Lejeune, and Mahaux [36] is adopted for the calculations. The OMP's of Becchetti and Greenlees [37] and Bauge, Delaroche, and Girod [38] lead to an overprediction of the experimental data over the whole energy range. The comparison between data and theoretical predictions revealed that the HF calculations are very sensitive to both neutron and proton OMP's over the entire energy range. On the other hand, significant differences in the NLD's that were used are observed mainly at large energies.

The results of the present work suggest further cross-section measurements of (p,γ) reactions in the mass region considered, in order to derive the systematics needed for a globalization of the nuclear input parameters of the HF calculations.

ACKNOWLEDGMENTS

This work was supported by the NATO Collaborative Research Grants Programme (Contract No. CRG961086). C.A. acknowledges the support by the program P4/18 on interuniversitary attraction poles of the Belgian State Federal Service for Scientific, Technical and Cultural Affairs. T. R. acknowledges the support of the Swiss National Science Foundation (Grants No. 2124-055832.98 and No. 2000-061822.00).

[1] F. Käppeler, F.-K. Thielemann, and M. Wiescher, Annu. Rev. Nucl. Part. Sci. **48**, 175 (1998).
[2] W. Hauser and H. Feshbach, Phys. Rev. **87**, 366 (1952).
[3] P. A. Seeger, W. P. A. Fowler, and D. D. Clayton, Astrophys. J., Suppl. **11**, 121 (1965).
[4] F. Käppeler, H. Beer, and K. Wisshak, Rep. Prog. Phys. **52**, 945 (1989).
[5] B. S. Meyer, Annu. Rev. Astron. Astrophys. **32**, 153 (1994).
[6] M. Arnould, Astron. Astrophys. **46**, 117 (1976).
[7] M. Rayet, M. Arnould, M. Hashimoto, N. Prantzos, and K. Nomoto, Astron. Astrophys. **298**, 517 (1995).
[8] M. Arnould, M. Rayet, and M. Hashimoto, in *Unstable Nuclei in Astrophysics*, edited by S. Kubono and T. Kajino (World Scientific, Singapore, 1992), p. 23.
[9] S. E. Woosley and W. M. Howard, Astrophys. J., Suppl. **36**, 285 (1978).
[10] N. Prantzos, M. Hashimoto, M. Rayet, and M. Arnould, Astron. Astrophys. **238**, 455 (1990).
[11] S. E. Woosley and T. A. Weaver, Astrophys. J., Suppl. **101**, 181 (1995).
[12] A. Heger, R. D. Hoffman, T. Rauscher, and S. E. Woosley, in *Proceedings of the X Workshop on Nuclear Astrophysics*, edited by W. Hillebrandt and E. Müller (MPA, Garching, 2000), p. 105.
[13] T. Rauscher, A. Heger, R. D. Hoffman, and S. E. Woosley, Nucl. Phys. **A688**, 193c (2001).
[14] V. Costa, M. Rayet, R. A. Zappalà, and M. Arnould, Astron. Astrophys. **358**, L67 (2000).
[15] S. M. Asida and D. Arnett, Astrophys. J. **545**, 435 (2000).
[16] C. E. Laird, D. Flynn, R. L. Hershberger, and F. Gabbard, Phys. Rev. C **35**, 1265 (1987).
[17] T. Sauter and F. Käppeler, Phys. Rev. C **55**, 3127 (1997).
[18] J. Bork, H. Schatz, F. Käppeler, and T. Rauscher, Phys. Rev. C **58**, 524 (1998).
[19] F. R. Chloupek, A. StJ. Murphy, R. N. Boyd, A. L. Cole, J. Görres, R. T. Guray, G. Raimann, J. J. Zach, T. Rauscher, J. V. Schwarzenberg, P. Tischhauser, and M. C. Wiescher, Nucl. Phys. **A652**, 391 (1999).
[20] S. Harissopulos, S. Galanopoulos, P. Tsagari, P. Demetriou, G. Kuburas, T. Paradellis, R. Kunz, J. W. Hammer, R. Kunz, G. Gyürky, E. Somorjai, S. Goriely, S. Kasemann, A. Dewald, and K. O. Zell, Nucl. Phys. **A688**, 421 (2001).
[21] G. Gyürky, E. Somorjai, T. Rauscher, and S. Harissopulos, Nucl. Phys. **A688**, 90 (2001).
[22] N. Özkan, A. StJ. Murphy, R. N. Boyd, A. L. Cole, R. de Haan, M. Famiano, J. Göerres, R. T. Güray, M. Howard, L. Sahin, and M. Wiescher, Nucl. Phys. **A688**, 459 (2001).
[23] E. Somorjai, Zs. Fülöp, A. Z. Kiss, C. Rolfs, H-P. Trautvetter, U. Greife, M. Junker, M. Arnould, M. Rayet, S. Goriely, T. Rauscher, H. Oberhummer, and P. Mohr, in *Nuclei in the Cosmos V*, edited by N. Prantzos and S. Harissopulos (Editions Frontières, Paris, 1998), p. 459.
[24] Zs. Fülöp, A. Z. Kiss, E. Somorjai, C. E. Rolfs, H. P. Trautvetter, T. Rauscher, and H. Oberhummer, Z. Phys. A **355**, 203 (1996).
[25] W. Rapp, H. J. Brede, M. Heil, D. Hentschel, F. Käppeler, H. Klein, R. Reifrath, and T. Rauscher, Nucl. Phys. **A688**, 427 (2001).
[26] R. Kunz, M. Jaeger, A. Mayer, J. W. Hammer, G. Staudt, S. Harissopulos, and T. Paradellis, Phys. Rev. Lett. **86**, 3244 (2001).
[27] J. C. Sens, S. M. Refaei, and A. Pape, Phys. Rev. C **18**, 2007 (1978).
[28] H. H. Andersen and J. F. Ziegler, *Hydrogen Stopping Powers and Ranges in All Elements* (Pergamon, New York 1997), Vol. 3.
[29] S. Goriely, in *Nuclei in the Cosmos V*, edited by N. Prantzos and S. Harissopulos (Editions Frontières, Paris, 1998), p. 314 (see also http://www-astro.ulb.ac.be).
[30] T. Rauscher and T.-K. Thielemann, At. Data Nucl. Data Tables **75**, 1 (2000).
[31] P. Demetriou and S. Goriely, Nucl. Phys. **A688**, 584 (2001).

[32] P. Demetriou and S. Goriely, Nucl. Phys. **A695**, 3 (2001).
[33] S. Goriely, Nucl. Phys. **A605**, 28 (1996).
[34] T. Rauscher, F.-K. Thielemann, and K.-L. Kratz, Phys. Rev. C **56**, 1613 (1997).
[35] P. Möller, J. R. Nix, W. D. Myers, and W. J. Swiatecki, At. Data Nucl. Data Tables **59**, 185 (1995).
[36] J. P. Jeukenne, A. Lejeune, and C. Mahaux, Phys. Rev. C **16**, 80 (1977).
[37] F. D. Becchetti and G. W. Greenlees, Phys. Rev. **182**, 1190 (1969).
[38] E. Bauge, J. P. Delaroche, and M. Girod, Phys. Rev. C **63**, 024607 (2001).